Wideband System-Level Simulator for Passive UHF RFID

Daniel Arnitz†, Ulrich Muehlmann‡, Thomas Gigl†, and Klaus Witrisal†

† Signal Processing and Speech Communication Laboratory, Graz University of Technology, Graz, Austria
{daniel.arnitz, thomas.gigl, witrisal}@tugraz.at
‡ NXP Semiconductors, Gratkorn, Austria
ulrich.muehlmann@nxp.com

***Abstract*—A chip manufacturing process requires extensive support of CAD-tools in order to predict the behavior of the embedded circuitry and to ensure the intended system functionality. Past experience shows that the overall performance of UHF RFID systems is mainly limited by multipath propagation and detuning. In this context, system-level simulations are vital to assess the overall performance and improve the embedded circuit. We present a simulator framework capable of handling chip-level tag models, fading MIMO radio channels, and interrogator building blocks on signal level. It is based on highly flexible behavioral tag-models instead of highly accurate but static ASIC models. In contrast to other UHF RFID simulators, it is explicitly designed to handle wideband signals, fading channels, nonlinearities, and detuning effects. The simulator is currently used to develop and evaluate the performance of ranging and realtime channel estimation systems. The presented results emphasize the feasibility of our framework in the evaluation of a range estimation approach between a standard UHF RFID transponder and an interrogator.**

***Index Terms*—UHF RFID, system modeling, nonlinear systems, simulation, wideband channel, multipath channel, detuning, ranging**

I. Introduction

Current developments in UHF RFID are mostly driven by cheaper transponder chip implementations and by increasing the read range (cf. [1]). These are market relevant aspects, since in 2005 and 2006 major retailers announced to replace barcodes by RFID tags [2]. It is an open secret that multipath propagation and detuning are significant challenges in this process. Consequently, average performance in multipath environments became a major issue.

In order to estimate the performance of existing implementations and to accelerate and simplify development processes, simulation tools for passive UHF RFID [3]–[5] were explicitly designed to analyze state-of-the-art systems. As spectral masks and permitted frequency bands are quite strict ([2], [6]), these simulation architectures only feature narrowband models. Furthermore, just the simulator presented in [4] supports fading channels. Although a narrowband assumption is an obvious choice for the analysis of today's systems, next generation RFID might take advantage of the benefits of wideband and multiband systems in multipath environments.

The presented simulator framework is specifically designed to support the development and verification of wideband and ultra-wideband (UWB) system components in fading environments. Furthermore, it is designed to handle arbitrary tag properties, which cannot be provided by ASIC simulators like the architecture described in [3].

This document is organized as follows: Section II gives an overview over the simulator structure and its purpose, while Section III lists more specific details about the implementation and limitations. Current simulation examples can be found in Section IV. This Section also contains a signal model used for these simulations and a brief outlook on future improvements. Note that some parts of Section IV-A, including Fig. 7, appear in [7].

II. Overview: General Structure / Framework

A. Field of Application

The presented simulator is primarily designed to study new system components that are far beyond state-of-the-art technology or require reader/tag performance that can not be achieved yet. As a key differentiator to other simulators as proposed in [3]–[5], it is designed to handle wideband signals in the presence of nonlinearities, fading, and detuning. Sophisticated approaches like combined frequency-/time-domain simulation [3] are difficult to handle and provide little gain in terms of simulation performance under such circumstances. Accordingly, our simulator is based on a straightforward sampled time-domain approach written in Matlab.

Complexity is the major drawback of this implementation: Due to the UHF ($\sim$GHz) carrier and low data rates ($\sim$kHz), RAM usage is extensive. Block processing (cf. Fig. 1) is applied to mitigate this drawback. The blocksize is variable and typically chosen to be one data burst (e.g., a single command). Performance problems limit the use of this architecture for protocol simulations (e.g., anticollision). However, such simulations are not the primary field of application for this simulator.

Currently the system is used to develop and test realtime channel estimation systems in fading and nonfading environments; examples can be found in Section IV. Connected to that problem is a major issue of the past years: ranging.

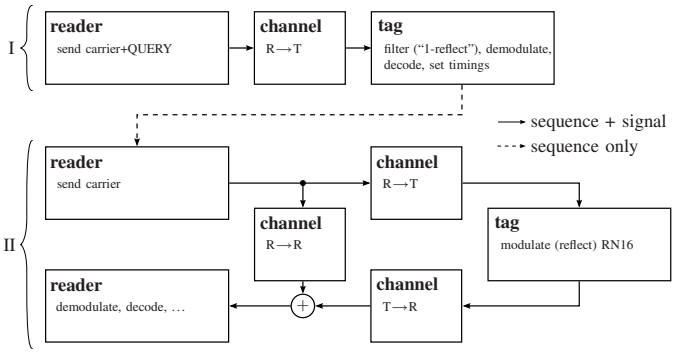

Fig. 1. Block processing example (EPCglobal Class-1 Gen-2 protocol [8]). Block I: The interrogator (reader) sends a QUERY command to the tag. Block II: The tag answers with RN16, i.e., modulates a carrier that has been generated by the reader. The signals are transmitted over reader→reader and reader↔tag channels. In general, multiple readers/channels/tags are handled.

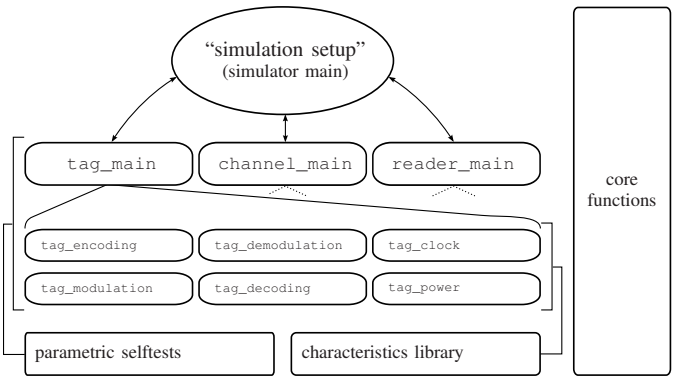

Fig. 2. Basic simulator structure: The complex bottom-level functions (`reader_*`, `channel_*`, `tag_*`) are handled by simple top-level interfaces (`*_main`); the user can construct the "simulation setup" in an interpreter fashion. All modules are verified by parametric selftests; core functions manage function/characteristic versions, logging and exceptions.

B. Structure Overview

The simulator is organized in two abstraction levels (see Fig. 2) to simplify its handling. Top-level functions (`*_main`) provide a simple interface for the user to build custom simulation setups (e.g., a EPCglobal Gen-2 [8] protocol simulation in a dense reader environment), while bottom-level functions (`reader_*`, `channel_*`, `tag_*`) perform the actual operations. In that fashion even complex protocols and/or simulation setups can be simplified to a few lines of code, making the creation of new setups a matter of minutes. The main script for the sequence shown in Fig. 1, for example, might look like this:

```
% issue QUERY command
r_tx = reader_main('query');
t_rx = channel_main('r->t', r_tx);
       tag_main(t_rx, 'query');
% reply RN16
r_tx = reader_main('carrier');
t_rx = channel_main('r->t', r_tx);
t_tx = tag_main(t_rx, 'rn16');
r_rx = channel_main('r->r',r_tx)+channel_main('t->r',t_tx);
       reader_main('rn16', r_rx);
```

Most components, especially the tag building blocks, use lookup tables to model their behavior. These tables form the characteristics library. The library is able to support different reader/tag types, although currently, it only holds the characteristics of one type of tag and a basic reader.

Administrative work is done by several background modules of the simulator, called core functions. This set of functions handles exceptions, and performs version control and logging. Furthermore, all major functions contain a parametric selftest. These tests verify that all functions work within a set of predefined parameters and thus ensure proper functionality of the entire simulator, for example, after modifications.

III. Implementation Details

The presented simulation environment has originally been designed for ranging simulations, without emphasis on the implementation details of an interrogator. Hence, most effort has been spent on tag and channel models.

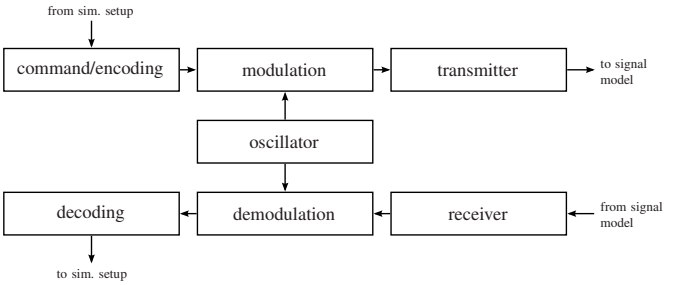

Fig. 3. Reader block diagram. Each reader in multireader environments is treated separately. Signal model and simulation setup are defined by the user in the "simulator main" script. A possible signal model is shown in Fig. 6.

In this Section, the "simulation setup" represents an overall metalevel of a specific simulation, defined in the simulator main script (cf. Fig. 2). Hence "sim. setup" in Figs. 3 and 5 is a synonym for the simulated physical setup (e.g., tags moving through a gate), the communications protocol (e.g., EPCglobal Gen-2), additional signal processing algorithms (e.g., ranging) and other high-level functions like user interaction.

A. Interrogator (see Fig. 3)

As mentioned above, the interrogator is implemented in a simple and straightforward manner. The oscillator produces a sine wave with arbitrary amplitude and phase instability, plus additive noise. This signal can be modulated according to the EPCglobal Class-1 Gen-2 standard [8] with cosine rolloffs. Arbitrary wideband carrier signals are also possible. The transmitter contains a nonlinear power amplifier and a linear bandpass model of the antenna.

The receive path consists of a bandpass filter plus a power splitter (receiver), and a standard zero-IF IQ demodulator with complex output. This output is filtered, re-sampled, and quantized (anti-aliasing-filter plus analog to digital conversion).

Encoding and decoding do not necessarily imply a communications protocol like EPC Gen-2 in this context. For example, these blocks could also represent a ranging method like the modulation and analysis of UWB pulses.

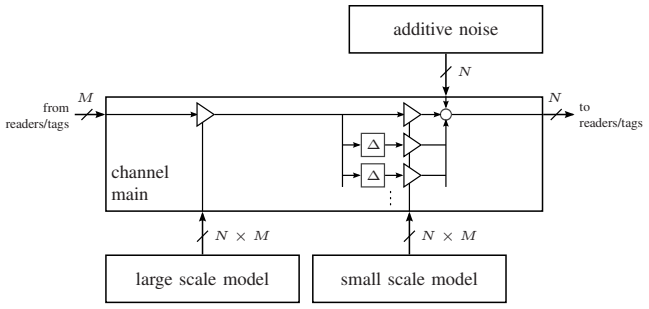

Fig. 4. Channel block diagram. Unlike reader and tag, the channel is XIXO per definition (e.g. M readers, N tags). Also the reader to reader channel $K(\omega, i)$ in Fig. 6 is modeled in this fashion ($M = N$ readers).

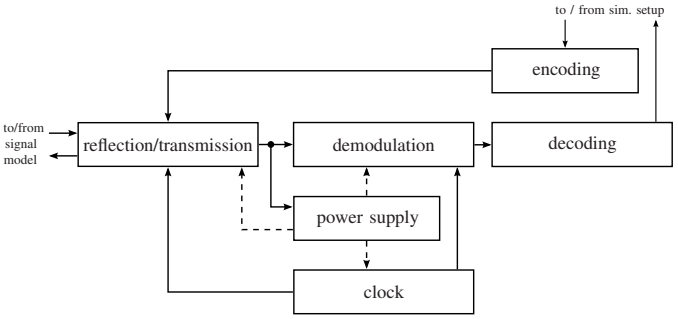

Fig. 5. Tag block diagram. Each tag in multitag environments is treated separately. Signal model and simulation setup are defined by the user in the "simulator main" script. A possible signal model is shown in Fig. 6.

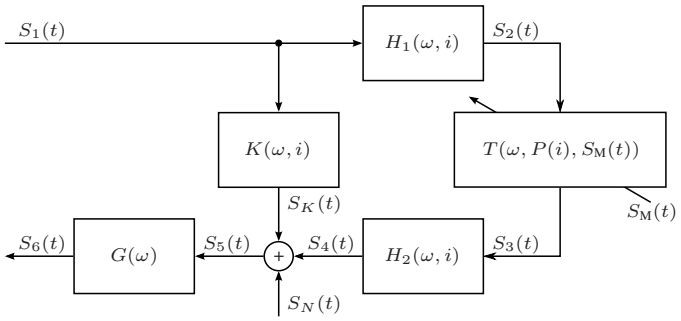

Fig. 6. Used signal model: Reader to reader channel $K(\omega, i)$, reader to tag channels $H_1(\omega, i)$ and $H_2(\omega, i)$, tag reflection coefficient $T(\omega, P, S_\mathrm{M})$, reader input stage $G(\omega)$, modulation signal $S_\mathrm{M}(t)$, carrier level signals $S_1(t)$ through $S_6(t)$, noise $S_N(t)$; i is the block index ($\rightarrow$ block processing), ω is the angular frequency, t is the time variable within one block

B. Channel (see Fig. 4)

In order to allow the application of standard wireless models, a linear channel has to be isolated. Spectral shaping by the reader may be (partially) located before the nonlinear power amplifier in the transmit path and is thus not included in the channel model. In order to keep the symmetry, spectral shaping in the reader's receive path is also excluded. Finally, the tag's reflection coefficient is also nonlinear and thus not covered by the channel model. Accordingly, the downlink channel starts after the power amplifier and stops at the reflection coefficient. The other direction – the uplink channel – starts at the reflection coefficient and ends at the reader's power splitter. As mentioned above, all channel models and their implementations are XIXO (arbitrary number of inputs and outputs) and wideband.

More precisely, the channel between two devices (e.g., reader/tag or reader/reader) consists of additive noise, a large-scale and a small-scale model. The large-scale channel consists of a log-distance model with optional log-normal shadowing. The small-scale model implements a sampled version of the average power-delay-profile described in [9] (model for short-range indoor radio channels) with $\tau_1 = 0$. This model creates Ricean fading characteristics for a single narrowband carrier. The small-scale channel can be configured to use a randomized or fixed power delay profile to model time-variant or time-invariant environments.

C. Tag (see Fig. 5)

The entire observable behavior of the tag at signal level is based on its reflection properties. This is why the reflection coefficient model is considered to be the most important part for the assembly of an accurate tag model. It is calculated using measured and simulated chip and antenna data and encompasses chip input impedance, modulation impedance, antenna impedance, as well as detuning. This nonlinear (incident power dependent), time-variant (modulation) and frequency dependent (resonances) reflection coefficient is implicitly linearized for one block by the assumption of a short-time stationary power, and modeled by a time-variant linear filter using a polyphase filterbank [10]. A more detailed study of a nonlinear implementation is currently conducted. Note that detuning is not covered directly by the simulator, but implicitly by selecting an appropriate reflection coefficient data set. This way the functionality of the simulation framework is independent of a specific detuning model.

Demodulator and power supply unit are based on lookup tables stored in the characteristics library. The clock source features arbitrary frequency instability and random initial phase. Decoding and encoding are implemented according to the Gen-2 protocol [8]; all other blocks have been modeled using data provided by NXP Semiconductors.

IV. Simulation Examples / Future Work

A. Signal Model and Linearized Tag Model

The signal model currently used for simulations is shown in Fig. 6. This drawing is limited to the communication between one reader and one tag for simplicity; the simulator supports multiple interrogators and multiple tags. Note that the signal model is a part of the simulator main script and thus defined by the user. All blocks except the tag reflection coefficient are assumed to be short-time stationary for one block index i ($\rightarrow$ block processing).

The reader to reader channel $K(\omega, i)$ and the uplink and downlink channels $H_2(\omega, i)$ and $H_1(\omega, i)$, respectively, are modeled as linear filter channels; ω is the angular frequency. $K(\omega, i)$ includes direct coupling as well as multipath feedback. The tag reflection coefficient $T(\omega, P(i), S_\mathrm{M}(t))$ is modulated

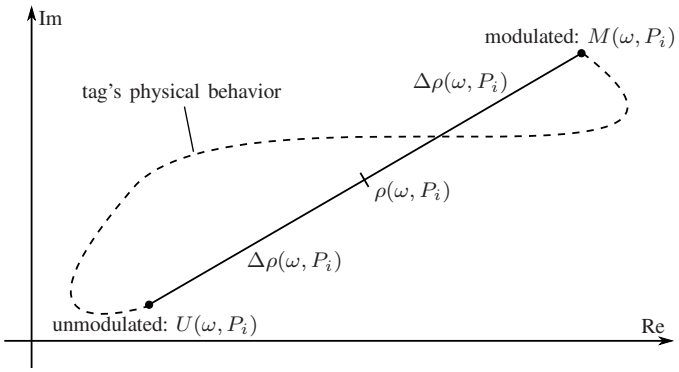

Fig. 7. Tag reflection coefficient linearization: The tag's physical behavior during modulation is a nonlinear, time-variant, frequency- and power-dependent curve. The linearized model assumes a fictive center value $\rho(\omega, P_i)$ and a difference value $\Delta\rho(\omega, P_i)$; only the endpoints are identical to the original curve. The assumption of short-time stationary power $P(i)=P_i$ completes the linearization.

by $S_{\mathrm{M}}(t)$ and, due to the assumption of short-time stationary power $P(i)$, implicitly linearized as follows:

On a physical level, the tag modulates data by varying a modulation impedance. The reflection coefficient during this process depends on the chip impedance, which itself depends on the chip input power. This dependence causes the reflection coefficient to be nonlinear. Furthermore, the interaction between the time-variant impedances creates a curved transition trajectory in the complex plane (cf. Fig. 7). The linearization now first neglects everything but the end points of this curve, introducing a center value $\rho(\omega, P)$ and a difference value $\Delta\rho(\omega, P)$. The end points are more important here than the trajectory itself, because of the nearly square tag modulation (either modulated or unmodulated).

$$\begin{aligned} \text{modulated:} \quad & M(\omega, P) = \rho(\omega, P) + \Delta\rho(\omega, P) \\ \text{unmodulated:} \quad & U(\omega, P) = \rho(\omega, P) - \Delta\rho(\omega, P) \end{aligned} \tag{1}$$

Assuming an arbitrary modulation signal $S_{\mathrm{M}}(t)$ satisfying $-1 \leq S_{\mathrm{M}}(t) \leq 1$ we can approximate the time-variant tag reflection coefficient $T(\omega, P, t)$ by

$$T(\omega, P, S_{\mathrm{M}}(t)) \approx \rho(\omega, P) + S_{\mathrm{M}}(t) \cdot \Delta\rho(\omega, P) \tag{2}$$

which is a simplified trajectory, but still power-dependent and thus nonlinear. Assuming short-time-stationary power (one block) $P \to P(i)$, the linearization is complete

$$T(\omega, P(i), S_{\mathrm{M}}(t)) \approx \rho_i(\omega) + S_{\mathrm{M}}(t) \cdot \Delta\rho_i(\omega) \tag{3}$$

By assuming a symmetrical and zero-mean modulation (like, for instance, a cosine), the center value ρ is identical to the average reflection coefficient. As mentioned above, the tag's reflection coefficient is implicitly linearized by the assumption of short-time stationary power.

B. Signal (+ Channel) Model Estimation

A typical characterization of the UHF RFID channel is focused on narrowband signal analyses and receive power

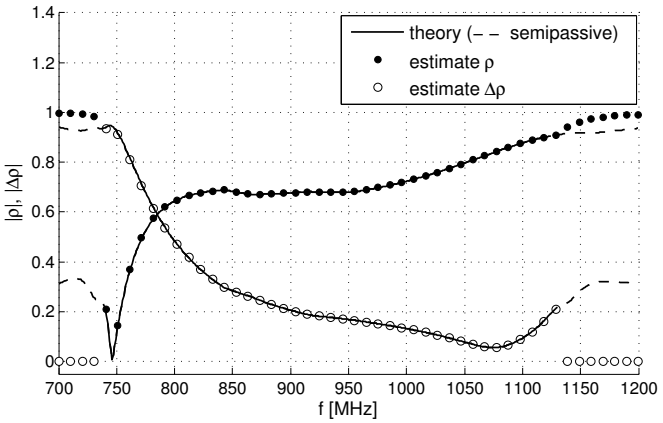

(a) magnitude

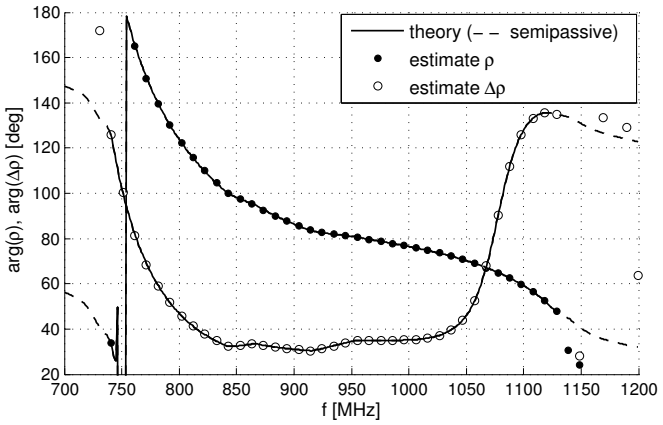

(b) phase

Fig. 8. Example: Signal model estimation. A linear model of the tag's reflection coefficient is estimated for one power level. Estimation window 2 ms per frequency, 100 kHz modulation frequency, AWGN channels with known distances, feedback attenuation 32 dB, additive noise −82 dBm/Hz, passive tag (functional, i.e., powered and continuous modulation possible within approx. 740−1125 MHz), typical assembly/detuning.

measurements (e.g., [11]–[14]). Short-range (< 10 m) wideband channel measurements in the UHF frequency band are rare ([15], cf. [16]–[18]). To our knowledge, wideband channel measurements with typical UHF RFID setups (like gates) are not publicly available in the literature.

Although a narrowband model is sufficient for product development based on current standards and regulations, it is limiting for research on next generation products. For instance, ranging methods typically require a significant amount of bandwidth to mitigate multipath interference effects. As a consequence, narrowband models are not suitable, hence the creation of a wideband channel model for UHF RFID is of vital importance to this simulator and all related applications. For example, the distance between interrogator and tag is an inherent channel property. Estimating this distance (ranging) is therefore identical to a channel estimation.

Currently, and as a pilot test prior to measurements, the simulator is used to test methods to estimate and separate channel from tag characteristics. A challenge for such an

estimation is the nonlinearity of the reflection coefficient and the fact that power measurements on passive tags are not feasible, especially during normal operation. Any outside observer, for instance, the interrogator, can only measure incident plus reflected power. As the reflection coefficient and thus the reflected power depends on the incident power, the inference from observed on incident power levels is ambiguous. For example, an observed power level of 1 mW could be created by 1 mW incident power without reflection (perfect matching) or by 0.5 mW incident plus 0.5 mW reflected power.

These simulations are based on the signal model shown in Fig. 6; a first result is shown in Fig. 8: Assuming known AWGN channels, the linear model of the tag's reflection coefficient, consisting of the average reflection coefficient ρ and the difference value $\Delta\rho$, is estimated by hopping the carrier frequency. The hopping creates short-time stationary power levels, thus eliminating the nonlinearity of the reflection coefficient. Subsequently the linear model is a perfect match, which is underlined by the simulation results in Fig. 8; the effect of additive noise is negligible for the used window size of 2 ms. The modulation stops outside $740-1125$ MHz, indicating that the tag reflects too much power to stay operational. Detuning would diminish this frequency range and shift it towards lower frequencies, thus the result corresponds well with the intended minimal frequency range of $840-960$ MHz for moderately detuned tags.

Once its reflective properties are known, the tag is placed into a multipath environment. By continuously estimating the frequency response of the system, wideband channel properties can be obtained.

C. Ranging

The first application to test the capabilities of the simulator was multi-frequency continuous-wave radar ranging [7], a generalization of [19].

As an example, a tag is placed at a distance of $0.5, 1, 1.5, \ldots 4$ m from the interrogator. This range is then estimated multiple times per distance setting using two-frequency continuous-wave radar. The theoretical bounds for the distance error's variance and the expected average error are derived in [7]. Under the assumption of an AWGN channel and a perfectly calibrated reader input stage, we can write

$$\begin{aligned} \mathrm{E}\left\{\widetilde{d}\right\} &= \frac{c}{2\omega_1}\left(\angle\Delta\rho_2 - \angle\Delta\rho_1\right) \\ \mathrm{var}\left\{\widetilde{d}\right\} &\approx \frac{c^2 N_0}{16 N \omega_1^2} \cdot \frac{1}{|A_1|^2 |H_1|^4 |\Delta\rho_1|^2} \\ &\quad + \frac{c^2 N_0}{16 N \omega_1^2} \cdot \frac{1}{|A_2|^2 |H_2|^4 |\Delta\rho_2|^2} \end{aligned} \tag{4}$$

for the distance error $\widetilde{d}$, where c is the speed of light, N_0 is the single-sided noise density, N is the number of averaged samples, ω_1 is the offset frequency between main and secondary carrier, H is the channel gain, A is the carrier amplitude and $\Delta\rho$ is the differential linearized reflection coefficient. Index 1 denotes the main carrier while 2 indicates the secondary carrier. The simulation result is shown in Fig. 9.

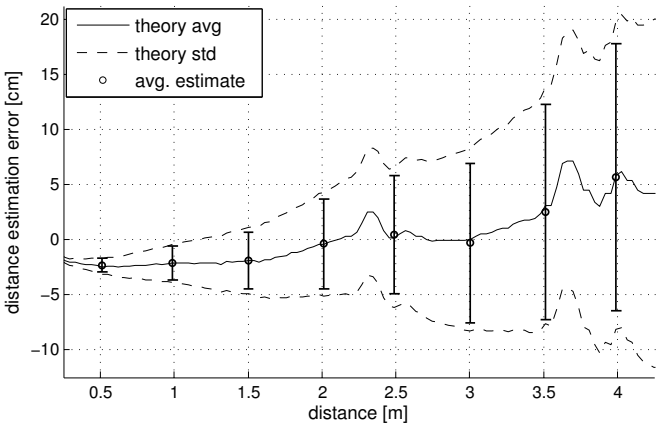

Fig. 9. Example: Two-frequency continuous-wave radar ranging; AWGN channel, single-sided noise density $N_0 = -82$ dBm/Hz, isotropic carrier power 1 W/10 mW for primary/secondary carrier, frequency spacing 1 MHz, typical tag/assembly. Errorbars represent mean and standard deviation of 500 realizations per distance setting $(0.5, 1, 1.5, \ldots, 4\,\mathrm{m})$.

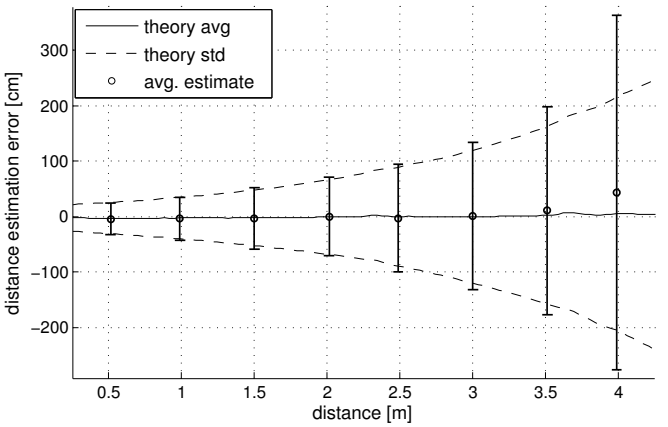

Fig. 10. Example: Two-frequency continuous-wave radar ranging; noiseless fading channel, logarithmic trends for Ricean K-factor K=30...10 dB and RMS delay spread $\tau_{RMS} = 1...20$ ns within distance 0...5 m (per channel). Isotropic carrier power 1 W/10 mW for primary/secondary carrier, frequency spacing 1 MHz, typical tag/assembly. Errorbars represent mean and standard deviation of 500 realizations per distance setting $(0.5, 1, 1.5, \ldots, 4\,\mathrm{m})$. Note that the exponential behavior is mainly due to the logarithmically changing K and τ_{RMS}.

Using the same ranging approach in a multipath environment, shown in Fig. 10, the standard deviation increases significantly. Like any narrowband system, two-frequency continuous-wave ranging is not able to mitigate multipath propagation effects. The only mitigating factor is the correlation between the channel frequency responses H_1 and H_2 at primary and secondary carrier frequency, respectively. The theoretical variance is [7]

$$\mathrm{var}\left\{\widetilde{d}\right\} \approx \frac{c^2}{8\omega_1^2} \cdot \frac{\mathrm{Re}\left\{\sigma^4 - \beta^2 + 2|m|^2\left(\sigma^2 - \beta\right)\right\}}{\mathrm{Re}\left\{\beta + |m|^2\right\}^2} \tag{5}$$

where σ^2 is the variance of the channel gains, β is the cross-covariance and m the expected value. This result assumes i.i.d. circular symmetric complex Gaussian channel gains for

primary and secondary carrier $H_1, H_2 \sim \mathcal{CN}(m, \sigma^2)$, which reflects a Ricean fading channel. Moreover, this approximation is only true for LOS-scenarios (high K-Factor).

D. Modifications to the Simulator

The present simulation architecture is still under development, adding and/or improving components on a need-to-have basis.

One of the weaknesses of the current implementation is the assumption of short-time stationary power conditions. Although fast changes in the incident power are filtered by the tag's power supply buffer, relatively slow changes w.r.t. the time constants of the tag power supply are not covered by this stationary model. Accordingly, the current reflection coefficient implementation will be replaced by a time-variant nonlinear approximation, allowing time-variant power levels.

Other future issues are more efficient implementations of filter channels and tag modulation, and of course the incorporation of the findings of the signal model and channel measurements described above.

V. Conclusion

In this paper, a system-level UHF RFID simulator based on behavioral models is described. This simulator is the first UHF RFID simulator to the authors' knowledge that supports (ultra)wideband signals as well as fading channels, different tag models, detuning, and nonlinearities at carrier level. Self-test routines ensure that all modules work within a predefined set of parameters and guarantee proper functionality of the complex simulator framework.

The simulator's tag-models are based on simulated and measured data of commercial UHF transponder chips. The most important signal-level property of the tag – the reflection coefficient – encompasses chip input impedance, modulation impedance, antenna impedance, and detuning. The channel is based on a wireless indoor power-delay-profile.

Two simulation examples are presented. The first example is a narrowband range estimation system based on a second carrier, the second example is a preliminary test simulation prior to channel/signal model measurements. The simulation results agree with wireless communications theory in both examples, underlining the validity of the simulator.

VI. Acknowledgments

The authors would like to thank NXP Semiconductors, Gratkorn, Austria, for funding this project and for providing data for the tag library. This work is supported by the national Austrian Research Promotion Agency (FFG) under the grant number 818072, for which we are also very grateful.

References

[1] "The RFID benchmark report - finding the technology's tipping point," Aberdeen Group, Dec. 2005.

[2] D. M. Dobkin, *The RF in RFID*. Elsevier, 2007, ISBN-13: 978-0750682091.

[3] V. Derbek, J. Preishuber-Pfluegl, C. Steger, and M. Pistauer, "Architecture for model-based UHF RFID system design verification," in *European Conference on Circuit Theory and Design (ECCTD05)*, vol. 2, Sept. 2005, pp. 181–184, 10.1109/ECCTD.2005.1523023.

[4] C. Floerkemeier and R. Pappu, "Evaluation of RFIDSim - a physical and logical layer RFID simulation engine," in *International Conference on RFID (RFID2008))*, Apr. 2008, pp. 350–356, 10.1109/RFID.2008.4519374.

[5] J. Li and C. Tao, "Analysis and simulation of UHF RFID system," in *International Conference on Signal Processing (ICSP2006))*, vol. 4, 2006, pp. 16–20, 10.1109/ICOSP.2006.346107.

[6] K. Finkenzeller, *RFID Handbook: Fundamentals and Applications in Contactless Smart Cards and Identification*, 2nd ed. Wiley & Sons, 2003, ISBN-13: 978-0470844021.

[7] D. Arnitz, K. Witrisal, and U. Muehlmann, "Multi-frequency continuous-wave radar approach to ranging in passive UHF RFID," to be published in IEEE Trans. Microwave Theory Tech.

[8] *ISO/IEC 18000-6C (EPCglobal Class 1 Gen 2)*, ISO Std., 2004.

[9] K. Witrisal, Y.-H. Kim, and R. Prasad, "A new method to measure parameters of frequency-selective radio channels using power measurements," *IEEE Trans. Commun.*, vol. 49, no. 10, pp. 1788–1800, Oct. 2001, 10.1109/26.957401.

[10] W. Lubberhuizen. (2007) Near perfect reconstruction polyphase filterbank. Matlab Central. [Online]. Available: http://www.mathworks.com/matlabcentral/fileexchange/15813

[11] D. Kim, M. A. Ingram, and W. W. Smith, "Measurements of small-scale fading and path loss for long range RF tags," *IEEE Trans. Antennas Propagat.*, vol. 51, no. 8, pp. 1740–1749, Aug. 2003, 10.1109/TAP.2003.814752.

[12] R. J. C. Bultitude, "Measurement, characterization and modeling of indoor 800/900 MHz radio channels for digital communications," *IEEE Commun. Mag.*, vol. 25, no. 6, pp. 5–12, June 1987.

[13] T. S. Rappaport and C. D. McGillem, "UHF fading in factories," *IEEE J. Select. Areas Commun.*, vol. 7, no. 1, pp. 40–48, Jan. 1989, 10.1109/49.16842.

[14] P. N. Nikitin and K. V. S. Rao, "Antennas and propagation in UHF RFID systems," in *International Conference on RFID (RFID2008)*, Apr. 2008, pp. 277–288, 10.1109/RFID.2008.4519368.

[15] M. S. Varela and M. G. Sánchez, "RMS delay and coherence bandwidth measurements in indoor radio channels in the UHF band," *IEEE Trans. Veh. Technol.*, vol. 50, no. 2, pp. 515–525, Mar. 2001, 10.1109/25.923063.

[16] T. Takeuchi, M. Sako, and S. Yoshida, "Multipath delay estimation for indoor wireless communication," in *Vehicular Technology Conference (VETEC1990)*, 1990, pp. 401–406, 10.1109/VETEC.1990.110355.

[17] T. S. Rappaport, *Wireless Communications*, 2nd ed. Prentice Hall International, 2002, ISBN-13: 978-0130422323.

[18] D. M. J. Devasirvatham, M. J. Krain, D. A. Rappaport, and C. Banerjee, "Radio propagation measurements at 850 MHz, 1.7 GHz and 4 GHz inside two dissimilar office buildings," *Electronics Letters*, vol. 26, no. 7, pp. 445–447, Mar. 1990, 10.1049/el:19900289.

[19] U. Muehlmann and A. Salfelner, "Two-frequency CW RADAR approach to ranging in UHF RFID systems," in *Proceedings of the European Microwave Association (EuMA07)*, vol. 4, Dec. 2007, pp. 317–322.